processes

MDPI

Article

Impact of TEMPO-Oxidation Pretreatment of Red Ginseng Residual on Nanofibrillation

Audrey Zahra, Virginia Ghita Firsty and Soo-Jeong Shin *

Department of Forest Product, Chungbuk National University Graduate School, Cheongju 28644, Republic of Korea
* Correspondence: soojshin@chungbuk.ac.kr

Abstract: Red ginseng extract is one of the most widely used herbal medicines to prevent and cure various diseases. Among the processed products derived from red ginseng, the water-insoluble part as red ginseng residual (RGR) becomes waste, even though it contains important ingredients. TEMPO-oxidation (TO) can be used as a pre-treatment with different degrees of oxidation (DO) (0 to 0.4) in red ginseng residual (RGR-TO) by introducing chemical oxidation and high-pressure homogenizer (HPH) as a nanofibrillation process. ^{1}H NMR was used to determine the carbohydrate composition and calculate DO, size was examined using a nanoparticle analyzer, and the zeta potential was used to determine surface charge density. RGR-TO with different concentrations had different compositions; glucose and uronic acid were the main ingredients. All treated RGR-TO showed higher oxidant levels than the untreated counterpart (RGR-TO 0). As the oxidant levels increased, the zeta potential and uronic acid increased, but the size of the nanofibril from RGR-TO decreased. The results of this study showed that TEMPO-oxidation pretreatment was effective in producing RGR cellulose nanofibril (CNF) with a variety of properties by adjusting the level of oxidation pretreatment and the number of HPH passes.

Keywords: red ginseng residual; TEMPO-oxidation; chemical oxidation; nanofibrillation

Citation: Zahra, A.; Firsty, V.G.; Shin, S.-J. Impact of TEMPO-Oxidation Pretreatment of Red Ginseng Residual on Nanofibrillation. *Processes* **2024**, *12*, 1035. https://doi.org/10.3390/pr12051035

Academic Editors: Ming-Hsun Cheng, Kurt A. Rosentrater, Amin Mirkouei, Ramkrishna Singh and Abraham Kabutey

Received: 13 March 2024
Revised: 14 May 2024
Accepted: 14 May 2024
Published: 20 May 2024

1. Introduction

Panax ginseng, also known as ginseng, is an herbaceous perennial plant that belongs to the *Araliaceae* family [1]. *Panax ginseng* Meyer has been used for over a thousand years in traditional Chinese, Korean, and Japanese medicine for its therapeutic benefits. This herb is also used as a functional food to maintain the body's balance and promote overall well-being [2,3]. Ginseng is renowned for its complex composition, which includes a variety of primary ingredients, such as ginseng saponins, volatile oil, amino acids, minerals, and vitamins [2,4]. These components work together to improve skin health by supplying essential nutrients, reducing cholesterol levels, encouraging blood circulation, and preventing arteriosclerosis [5]. Additionally, trace components found in ginseng help to enhance skin suppleness, reduce dry skin, and maintain moisture balance [6].

Ginseng is a crucial component of anti-aging and anti-oxidant medications, contributes to maintaining the skin's suppleness, and is often referred to as "wrinkles to return to Dan" due to its ability to improve the appearance of fine lines and wrinkles [6–8]. Red ginseng (RG) is a highly valued herbal supplement that is obtained by subjecting the root and rhizome of the *Araliaceae* plant to a unique process of steaming and drying [6]. It is frequently utilized as a cosmetic raw ingredient in China and the Republic of Korea for its brightening and anti-aging benefits. Its popularity in cosmetics is due to the fact that it helps to improve skin texture, reduce the appearance of fine lines and wrinkles, and promote a more youthful, radiant complexion [7,8].

In recent years, the use of red ginseng extract has become increasingly popular in the field of skincare due to its various benefits. This natural ingredient has been found to have a positive impact on the skin [9].

Recent studies have shown that red ginseng, a natural compound, contains specific monomer saponins such as Rb1, Rg1, CK, and Rg3 that offer several benefits to the skin. These compounds are believed to prevent the death of skin cells, known as keratinocytes, due to UV light exposure. They also promote the repair of DNA damage and stimulate the growth of new fibroblasts, which play a crucial role in tissue repair and wound healing [10]. Melanocytes in the skin produce melanin, a biopolymer that occurs naturally in the body [11]. While melanin is generally safe, excessive accumulation and overproduction of this compound can result in various skin problems, including pigment spots, chloasma, freckles, age spots, and even melanoma, a type of skin cancer. Maintaining a balance of melanin production is essential to avoid such physiological abnormalities [11,12].

Ginseng is a plant that contains a range of functional compounds that exhibit biological activity, including ginsenosides (saponin), peptides, polyacetylenes, alkaloids, and phenolic compounds, as well as acidic polysaccharides [13]. In Korea, raw ginseng is often processed to improve its efficacy and extend its storage period, resulting in two primary products: white and red ginseng [14]. Red ginseng is considered more potent than white ginseng due to its higher concentrations of specific ginsenosides, such as Rg3, Rh2, and Rb2 [15].

The most valuable processed product from red ginseng is its aqueous extract, which is highly applicable in the food industry [16]. This extract is obtained by boiling red ginseng in water or a mixture of water and ethanol, which recovers its water-soluble components, mainly consisting of ginsenosides and acidic polysaccharides [17]. The extraction process results in a water-insoluble by-product known as red ginseng residue (RGR), which is often discarded as waste. However, RGR contains components with biological activity, including acidic polysaccharides and lipid-soluble components, and has been found to be useful as a foodstuff and culture medium additive [15,18]. Therefore, it is important to consider the potential benefits of RGR in the food industry and explore ways to minimize waste.

Cellulose is a naturally occurring substance that can be found in various biological species, such as plants, animals, and some bacteria [19]. It is the primary building block of plants and is regarded as a valuable renewable resource that can replace petroleum-based materials [19–21]. There are several methods available for processing cellulose into nanomaterials, including high-pressure homogenization [22], microfluidization [23], grinding [24], cryocrushing [25], and high-intensity ultrasonication [26]. Additionally, cellulose can be pretreated by using various methods, such as enzyme treatment [27], carboxymethylation [28], acetylation [29], and TEMPO-oxidation [30]. These pretreatments modify the cellulose properties and enable the production of cellulose nanomaterials with unique characteristics.

The current research focuses on extracting cellulose in a nanodimensional structure, which can be further classified into different types such as cellulose nanofibrils (CNF), cellulose nanocrystals (CNC), and microfibrillated cellulose (MFC) [31]. The classification depends on the method of cellulose isolation [31]. CNF is produced by mechanical treatment of cellulose fibers, resulting in a highly fibrillated material [31]. Conversely, CNC is produced by acid hydrolysis of cellulose fibers, resulting in rod-like crystalline particles [31]. MFC is produced by mechanical treatment of cellulose fibers under conditions that promote the formation of a gel-like material that can be further processed into films, coatings, and composites [31].

Overall, the use of cellulose nanomaterials has gained significant attention due to their unique properties, including high specific surface area, high strength, and biodegradability. Researchers are exploring various applications of these materials in fields such as biomedicine, cosmetics ingredients, energy, and packaging.

Red ginseng is a highly sought-after natural remedy that offers numerous therapeutic benefits. However, its high cost has limited its accessibility to many individuals, and the presence of non-polar and volatile active ingredients has made it difficult to widely use [32,33]. The research aimed to convert solid residue from red ginseng into nanofibrillated products using TEMPO-oxidation. By analyzing the oxidation process meticulously and controlling the size of the nanofibril, the goal was to create an economical and better alternative product

compared to the remaining by-product that is typically used as animal feed or fertilizer. These findings offer valuable insights into the possibility of red ginseng residual as a cost-effective and efficient alternative to traditional red ginseng products.

2. Materials and Methods

2.1. Materials

Red ginseng residual (RGR) from the Korean Chungbuk Ginseng Cooperative (Jeungpyeong-gun, Republic of Korea) was used in this investigation (Figure 1). The RGR sample was ground using the IKA MF 10 basic Microfine grinder (IKA, Selangor, Malaysia) with an MF 2.0 sieve. There were several different chemicals used, including 2,2,6,6-Tetramethylpiperidine-1oxyl (TEMPO) from Aladdin Biochemical Technology Co., Ltd.; (Shanghai, China), sodium bromide (NaBr) from Samchun Pure Chemical Co., Ltd.; (Gyeonggi, Republic of Korea), sodium hypochlorite (NaClO) from Sungju Industrial (Gangjin, Republic of Korea); potassium hydroxide (KOH) from Samchun Pure Chemical Co., Ltd. (Gyeonggi, Republic of Korea); sulfuric acid (H_2SO_4) from Samchun Pure Chemical Co., Ltd. (Gyeonggi, Republic of Korea); and deuterium oxide (D_2O) from Sigma-Aldrich, Inc. (Darmstadt, Germany).

Figure 1. Red ginseng residual (**left**) and red ginseng residual after being ground (**right**).

2.2. Preparation of Red Ginseng Residual Nanoparticles in Different TEMPO-Oxidations

To initiate the TEMPO-oxidation reaction, a blend of RGR powder (100 g), TEMPO (0.5 g), and NaBr (2.5 g) was dissolved in distilled water. The mixture was constantly stirred while a NaClO (4%) solution was gradually added. The pH level was maintained at 10 throughout the process by adding 1M KOH until the KOH solution was no longer consumed. The whole oxidation process was carried out at room temperature for 4 h. Once the oxidation reaction was concluded, the resulting mixture was filtered, centrifuged, and washed multiple times with distilled water until the pH was neutral. This ensured that any unreacted chemicals were eliminated from the mixture.

To generate various RGR-TO samples with different target TO concentrations, three distinct RGR-TO samples were prepared. The target TO concentrations were set at 20 mM, 30 mM, and 40 mM, respectively. Each sample was subjected to TEMPO oxidation using different amounts of NaClO. The precise amounts of NaClO used were 3650 g, 5475 g, and 7300 g, respectively. These samples were then labeled as RGR-TO 1, RGR-TO 2, and RGR-TO 3, correspondingly.

The creation of hydrogel nanoparticles involves several steps. To begin, fibers that have undergone oxidation are mixed with distilled water until they reach a consistency of 2%. This mixture is then homogenized for 10 min using the IKA T25 Digital Ultra Turrax (Wertheim am Main, Germany), which runs at 8500 rpm to thoroughly break down the fibers. Next, the Panda PLUS 2000 high-pressure homogenizer (GEA, Parma, Italy) is used to produce the nanoparticles. This involves a series of treatments referred to as HPH-0, HPH-3, HPH-6, and HPH-9, with the machine run at a pressure of 400–600 bar and 0, 3, 6, and 9 passes, respectively. Finally, the nanoparticles are mixed with other ingredients

to produce a gel containing 2% RGR-TO hydrogel nanoparticles. The procedure for the experiment is outlined in Figure 2.

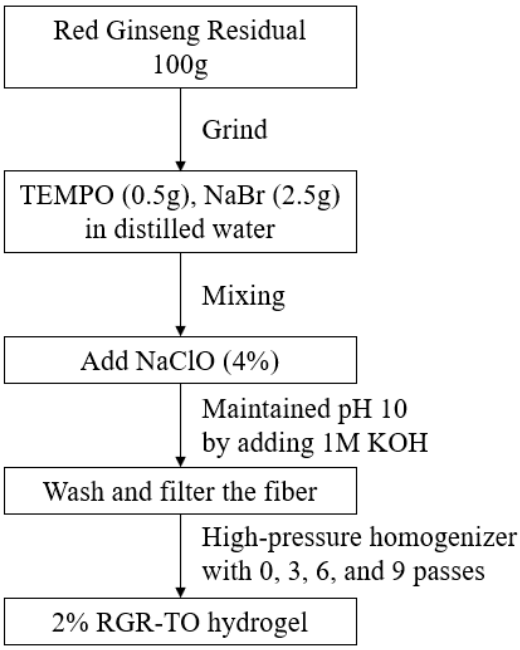

Figure 2. RGR-TO hydrogel process.

2.3. Analysis of Chemical Composition

A precise amount of 0.02 g of dried RGR-TO was weighed. Next, a precisely measured 0.6 mL of 72% H_2SO_4 was added to the sample. The mixture was then incubated at a temperature of 30 °C for one hour. After incubation, 3 mL of D_2O was added to the mixture and heated for an additional hour at 100 °C in the oven. Once cooled and filtered, the extractives were analyzed using a Bruker Avance 400 MHz ^{1}H-NMR (Bruker, Ettlingen, Germany). Each sample was repeated twice on average for accuracy. The goal of the experiment was to determine the composition of carbohydrates found in the sample.

Polysaccharides are complex molecules that are made up of repeating units of monosaccharides. When subjected to acid hydrolysis, the glycosidic bonds between the monosaccharide units are broken down, and the individual monosaccharides are released. These monosaccharides can be differentiated using ^{1}H-NMR spectroscopy. In ^{1}H-NMR, the anomeric hydrogen peak of each monosaccharide serves as a unique identifier, and the chemical shift of this peak distinguishes it from other monomers. The chemical shift acts like a fingerprint to identify each monomer. Each monosaccharide contains two anomeric hydrogens in alpha- and beta-forms, and their concentrations are proportional to the area under the peak, which is integrated using Bruker Topspin 3.6.3 NMR data analysis software.

The composition of each monomer is then calculated by adding the alpha and beta forms of each monosaccharide and multiplying the result by the molecule weight of each monosaccharide, and the total is then added up. The number of monosaccharides is multiplied by their molecule weight and divided by the total of all monosaccharides to make the carbohydrate-relative composition. This process allows for the exact compositional amount of each monosaccharide to be determined.

2.4. Degree of Oxidation Analysis

The degree of oxidation (DO) of RGR that was pretreated with TEMPO-oxidation was determined through analysis using a ^{1}H-NMR analyzer Bruker AVANCE NMR spectrometer (400 MHz). The Topspin program was used to integrate the data with anomeric hydrogen peaks and carboxyl group peaks on the spectrum. The integrated values were then

substituted into an equation to calculate the degree of oxidation of the TEMPO-oxidation pretreated red ginseng residual.

After the monosaccharide peak was identified and integrated and was quantitatively measured by calculating the area under the peak, the process was performed using Bruker Topspin 3.6.3 (software tool). The values obtained from this integration were then utilized to calculate the degree of oxidation (DO) of the red ginseng residue by using the equation below. The resulting DO value provides a quantitative measure of the extent to which the red ginseng residue has been oxidized.

$$DO = \frac{\alpha,\beta \text{ glucuronic acid in NMR peaks } - \alpha,\beta \text{ glucuronic acid in xylan before oxidation}}{\alpha,\beta\ glucose\ +\ \alpha,\beta\ glucuronic\ acid\ acid\ peaks\ in\ NMR\ -\ \alpha,\beta\ glucuronic\ acid\ in\ xylan}$$

2.5. Zeta Potential Measurement

RGR-TO samples were prepared for zeta potential analysis via dilution with distilled water to a concentration of 0.02%, followed by Zetasizer Nano ZS (Malvern, Worcestershire, UK) analysis at 25 °C. The data were derived for each sample using the average of three additional trials.

2.6. Nanoparticle Analysis

The sample was diluted with distilled water to a concentration of 0.02% and then processed with Zetasizer Nano ZS at 25 °C for nanoparticle analysis. According to ISO standard (ISO 22412:2008), size distribution findings were produced by averaging 10 consecutive measurements of 10–12 s runs [34].

2.7. Statistical Data Analyses

A comprehensive statistical approach was employed to analyze the data presented in Tables 1–3, utilizing Analysis of Variance (ANOVA), post hoc analysis with Tukey's Honest Significant Difference (HSD) test, and Pearson's correlation coefficient. Statistical differences between the means of groups across different levels of TEMPO oxidation and High-Pressure Homogenization (HPH) operation were assessed using ANOVA. For Tables 1 and 2, 4 groups representing different levels of TEMPO oxidation were analyzed. In Table 3, the analysis was extended to 12 groups, combining 3 different levels of TEMPO oxidation with 4 different levels of HPH operation. The comparison of the variation among group means with the variation within groups through ANOVA yielded an F-value, which was critical in determining the statistical significance of observed differences in means.

After identifying significant differences through ANOVA, a post hoc analysis was conducted using Tukey's HSD test. This step was essential for identifying specific pairs of group means that differed significantly. By this test being employed, pairwise comparisons between all possible group means were made, ensuring a thorough examination of the data.

Table 1. Monosaccharide composition of different TO-treated and untreated red ginseng residuals. Unit: (%).

Sample	Polysaccharide (%)							Degree of Oxidation (DO)
	Galactose	Arabinose	Glucose	Xylose	Mannose	Rhamnose	Uronic Acid (a + b + c)	
RGR-TO 0	4.84 ± 0.01	3.23 ± 0.01	77.64 ± 0.01	2.02 ± 0.02	1.08 ± 0.02	1.18 ± 0.01	10.15 ± 0.02	-
RGR-TO 1	3.83 ± 0.01	0.29 ± 0.02	71.90 ± 0.03	3.11 ± 0.01	1.36 ± 0.01	1.00 ± 0.02	18.62 ± 0.01	0.21 ± 0.02
RGR-TO 2	2.92 ± 0.02	0.36 ± 0.01	62.51 ± 0.02	3.19 ± 0.01	1.17 ± 0.02	0.00	29.86 ± 0.02	0.29 ± 0.02
RGR-TO 3	2.63 ± 0.03	0.37 ± 0.00	55.65 ± 0.01	2.79 ± 0.02	0.00	0.00	38.56 ± 0.01	0.37 ± 0.01

Table 2. Uronic acid composition of different TO-treated and untreated red ginseng residuals. Unit: (%).

Sample	* Glucuronic Acid (a)	Galacturonic Acid (b)	* Glucuronic ac. γ Lactone (c)
RGR-TO 0	8.26 ± 0.01	1.88 ± 0.02	0.00
RGR-TO 1	5.78 ± 0.00	2.15 ± 0.01	10.70 ± 0.01
RGR-TO 2	4.85 ± 0.02	3.93 ± 0.01	21.08 ± 0.02
RGR-TO 3	3.35 ± 0.03	3.40 ± 0.00	31.81 ± 0.01

* a and c are the same monosaccharide, glucuronic acid. However, during the hydrolysis for ^{1}H-NMR analysis, some of the glucuronic acid was degraded to glucuronic acid γ lactone.

Table 3. The particle size of RGR-TO.

Sample	High-Pressure Homogenizer (HPH)	Width (nm)	Length (nm)
RGR-TO 1	0	163.37 ± 5.71	1188.33 ± 38.11
	3	101.42 ± 7.59	727.80 ± 22.44
	6	77.87 ± 6.68	423.23 ± 13.34
	9	43.54 ± 6.11	230.37 ± 12.20
RGR-TO 2	0	138.70 ± 6.60	970.27 ± 15.28
	3	98.74 ± 7.13	656.07 ± 17.12
	6	67.40 ± 5.49	330.47 ± 20.38
	9	34.86 ± 7.94	169.07 ± 12.12
RGR-TO 3	0	124.97 ± 5.50	821.60 ± 23.73
	3	93.79 ± 4.48	557.23 ± 19.03
	6	57.86 ± 9.72	256.50 ± 11.92
	9	29.85 ± 7.56	121.03 ± 10.11

Pearson's correlation coefficient, denoted as r, was quantified to assess the strength and direction of the linear relationship between two continuous variables. With r ranging from −1 to +1, a perfect positive correlation is indicated by 1, a perfect negative correlation by −1, and no linear relationship by 0. This measurement is pivotal in understanding how closely data points cluster along a straight line. Across various fields, Pearson's r is extensively utilized to explore associations between variables, aiding in hypothesis testing and prediction. The relationships between different levels of TEMPO oxidation, HPH operation, and their combined effects on the variables of interest were thus explored.

3. Result and Discussion

3.1. Chemical Composition of Red Ginseng Residual Treated and Untreated TEMPO-Oxidation

The monosaccharide components in the red ginseng residual were characterized using ^{1}H NMR with different chemical shifts in anomeric hydrogen at 4.5–5.3 ppm [35–37] with the integrated peak area, as shown in Figure 3. The two main components of every RGR-TO sample were glucose and uronic acid, as shown in Tables 1 and 2. The amount of carboxyl groups increased with the concentration of dried RGR from the Republic of Korea that received TEMPO-oxidation pretreatment, which is evident from the percentage of uronic acid (Table 2). As the DO (degree of oxidation) increased, the amount of galactose, arabinose, glucose, and xylose decreased. Mannose was not identified at RGR-TO 3, and rhamnose was not observed at RGR-TO 2 and RGR-TO 3 (Table 1).

It was found that there were substantial variations in the composition of polysaccharides and the degree of oxidation after comparing the means across treatments. Significant differences in the polysaccharide composition ($F(3, 12) = 45.982$, $p < 0.001$) and degree of oxidation ($F(3, 12) = 65.365$, $p < 0.001$) among the treatments were indicated by ANOVA (analysis of variance). It was confirmed by post hoc Tukey's HSD tests that there were distinct polysaccharide compositions and oxidation degrees between treatments ($p < 0.05$).

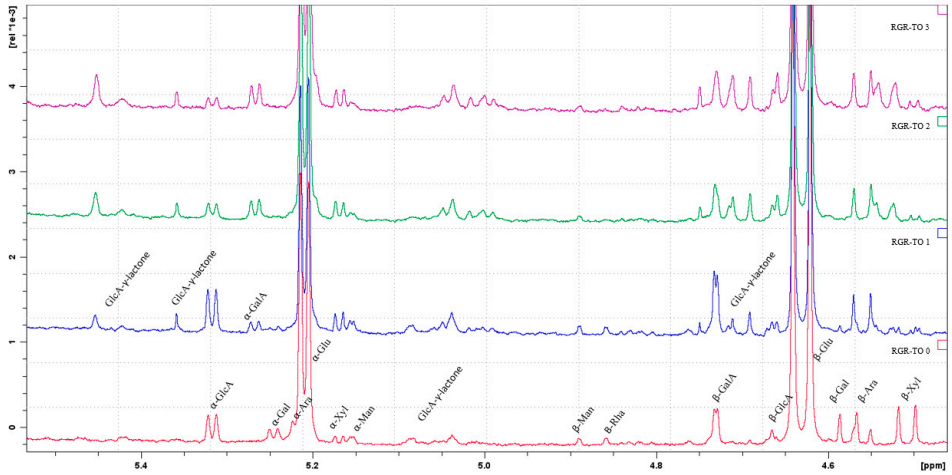

Figure 3. ^{1}H-NMR spectrum of monosaccharides from RGR-TO 0 (red), RGR-to 1 (blue), RGR-TO 2 (green), and RGR-TO 3 (purple).

Significant relationships were uncovered in the compositions of monosaccharides and uronic acids of red ginseng residuals through analysis. Between glucose and galactose in the monosaccharide composition, a strong positive correlation was observed (with r ranging from 0.974 to 0.991, $p < 0.01$), while a negative correlation with other monosaccharides was shown by xylose ($p < 0.01$). In the composition of uronic acids, a moderate negative correlation between glucuronic and galacturonic acids was noted (with r ranging from -0.730 to -0.889, $p < 0.05$). These findings reveal the structural changes and compositional dynamics occurring within red ginseng residuals under various treatment conditions.

Notable shifts in polysaccharide composition and oxidation levels across treatments were illustrated by trend analysis. Consistently, glucose content declined from RGR-TO 0 to RGR-TO 3, while uronic acid increased significantly. Progressively, galactose, arabinose, and mannose decreased, indicating structural alterations in polysaccharides. Conversely, xylose exhibited a transient increase followed by a decline, suggesting treatment-induced variations. Gradually, rhamnose diminished across treatments, potentially affecting ginseng's bioactive properties. The degree of oxidation displayed a linear increase, with glucuronic acid showing the most substantial rise, indicative of oxidation-induced modifications.

The impact of treatments on red ginseng residuals, significantly altering polysaccharide composition and oxidation levels, was highlighted by overall analysis. To elucidate ginseng's therapeutic properties and optimize its utilization in functional foods, cosmetics, and traditional medicine, understanding these changes is crucial.

Variations in the composition of polysaccharides and the degree of oxidation were found in the means across treatments. Significant differences in both polysaccharide composition and the degree of oxidation among treatments were revealed by ANOVA. Distinct compositions and oxidation between treatments were confirmed by post hoc Tukey's HSD tests. Interdependencies among polysaccharide components and the oxidation degree were suggested by correlation analysis. Notable shifts in composition and oxidation levels across treatments were shown by trend analysis. The impact of treatments on red ginseng residuals, altering composition and oxidation levels, was highlighted by these analyses.

Okara (soybean residue) from Beidahuang Green Health Food Co., Ltd. in Jiamusi, China, underwent TEMPO-oxidation treatment, which resulted in changes to its composition. Before treatment, it contained 1.23% glucuronic acid, 25.76% galacturonic acid, 7.69% galactose, 5.92% arabinose, 3.37% mannose, 6.79% rhamnose, 8.24% glucose, 6.16% fucose, and 34.84% xylose. However, after TEMPO-oxidation treatment, the composition changed to 0.98% glucuronic acid, 10.69% galacturonic acid, 38.14% galactose, 22.23% arabinose, 1.57% mannose, 3.89% rhamnose, 3.09% glucose, 3.73% fucose, and 15.76% xylose [35]. Similarly, xanthan from Jungbunzlauer in Basel, Switzerland, has 40 mol% glucose, 40 mol%

mannose, 20 mol% glucuronic acid, and 0 mol% mannuronic acid. Xanthouronan (named after TEMPO-oxidation) contains approximately ~1 mol% glucose, ~1 mol% mannose, 58.8 mol% glucuronic acid, and 39.2 mol% mannuronic acid [38]. The trend observed in both cases is that glucose and mannose levels decreased, while glucuronic acid and other uronic acids increased after the TEMPO-oxidation treatment, which is similar to the RGR-TO result.

Gluconic acid is a widely used active ingredient in cosmetic formulations that offers numerous benefits for human skin. This multifaceted substance functions as an exfoliant, anti-aging agent, moisturizer, and pH regulator, which collectively contribute to the overall health and appearance of the skin [39]. Its exfoliating properties work to eliminate dead skin cells and promote cellular regeneration, resulting in a smoother and more radiant complexion. Additionally, gluconic acid offers an effective anti-aging solution by minimizing fine lines and wrinkles, making it a popular ingredient in anti-aging skincare products [39,40]. Its exceptional moisturizing capabilities help to nourish and hydrate the skin, leaving it supple and revitalized. Lastly, the pH-regulating properties of gluconic acid are crucial in maintaining a healthy skin barrier, further contributing to the overall health and appearance of the skin [39].

Similarly, glucuronic acid is another widely used ingredient in cosmetic formulations, highly valued for its natural antioxidant properties. This substance is known to safeguard the skin from the damaging effects of free radicals, which are known to accelerate the aging process [41]. Additionally, glucuronic acid is a highly effective anti-aging agent that minimizes the appearance of fine lines and wrinkles, making it a valuable ingredient in anti-aging skincare products. Altogether, the combination of gluconic and glucuronic acids in cosmetic formulations can provide numerous benefits to the skin, promoting healthier and more youthful-looking skin [39–41].

3.2. Zeta Potential of Red Ginseng Residual-Treated and Untreated TEMPO-Oxidation

The zeta potential is essential in determining the surface charge density of nanomaterials, which in turn affects their dispersion stability in the media they are suspended in [42,43]. The zeta potential value of a suspension in water is a reliable indicator of its stability, with a value of 30 mV or more considered stable [43,44]. Additionally, the zeta potential value can determine the neutrality of a nanoparticle, with a value between −10 and +10 mV indicating neutrality. However, if the zeta potential value is more than +30 mV or less than −30 mV, the nanoparticle is considered strongly cationic or anionic, respectively [45]. It is important to note that the carboxyl group composition of each CNF can affect the correlation between the zeta potential and surface charge density [46].

The results of the zeta potential measurements showed that the addition of TEMPO-oxidation pretreatment significantly increased the zeta potential of the samples. For instance, the RGR-TO 0 (untreated) had a zeta potential value of −26.8 mV, while RGR-TO 3 (sample treated with DO 0.37) had a much higher negative charge of −74.8 mV, as shown in Figure 4. Similarly, CNF obtained from J. Rettenmaier & Sons, Holzmuhle, Germany, showed a similar trend, where the zeta potential values of TEMPO oxidatively dried hardwood kraft pulp supplemented with 0.7 mM, 1 mM, and 3 mM NaClO were −28.6 mV, −38.8 mV, and −51.9 mV, respectively [44]. Moreover, the CNF obtained from S. D. Fine Chemicals, Mumbai, India, had a zeta potential value of −20.36 mV for TO-CNF-B9 with the TEMPO oxidation method, while CNF without TEMPO pretreatment had a value of −14.16 mV [47]. Finally, the CNF from an oil palm empty fruit bunch (OPEFB), provided by HK Kitaran Sdn. Bhd. (Seberang Perai, Malaysia) after TEMPO pretreatment, had a zeta potential value of −45.4 mV [48]. Overall, the results indicate that the addition of TEMPO-oxidation pretreatment could potentially enhance the properties of the samples, leading to new opportunities for applications in various fields such as cosmetics, bio-composites, packaging materials, biomedical applications, water purification systems, and as functional additives in the paper and textile industries.

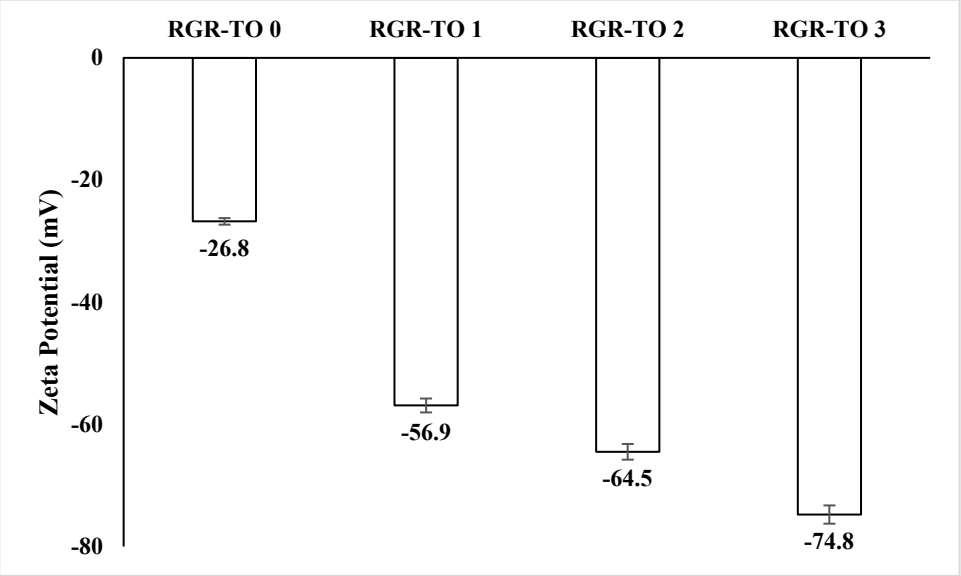

Figure 4. Zeta potential of different TO-treated red ginseng residual nanoparticles.

3.3. Size of Red Ginseng Residual-Treated and Untreated TEMPO-Oxidation

Table 3 shows that the size of RGR CNF nanoparticles decreased as the DO and HPH of the samples increased. This valuable insight was made possible through the innovative technique of nanoparticle sorting, which uses varying concentrations of DO and the number of HPH passes. This method could be customized to assess changes in hydrogel nanoparticle size, which is crucial for quality control and meeting regulatory aspects for enhancing the production of hydrogel-based products.

Efficient in-process quality control of cellulose nanofibrils is a crucial aspect of their production. To achieve this, a quick and straightforward method for assessing the size of the nanofibrils during the fabrication process is needed [49]. Researchers have found that utilizing a nanoparticle size analyzer that uses dynamic laser scattering is a reliable way to determine the length and width of the nanofibrils. During the characterization process, the dynamic laser scattering method produced two distinct peak regions for width and length [50].

Although the accuracy of the measurements taken from the nanoparticle analyzer was slightly less precise compared to those from TEM image analysis, both methods showed a consistent pattern in each sample [50]. It is suggested that despite the slightly less precise measurements, the dynamic laser scattering nanoparticle analysis method should be used as a quality-control technique to determine the length and width of cellulose nanofibers during fabrication [51]. This method provides a quick and easy way to assess the size of cellulose nanofibrils during the fabrication process. It can help manufacturers ensure that the final product meets the required size specifications, leading to consistent product quality.

Cellulose nanofibrils have a rod or linear structure with varying widths and lengths. Due to their large aspect ratio, the width ranges from several to several tens of nanometers, while the length ranges from hundreds to thousands of nanometers [24]. This large aspect ratio leads to cellulose nanofibers having different widths and lengths [52]. When used for nanoparticle size analysis, analyzing cellulose nanofibers can result in obtaining two or more particle size distributions rather than just one [53].

Notable differences in particle size can be elucidated by comparing means across treatments within each RGR-TO sample. Significant variations in both particle width and length among treatments within RGR-TO 1 (width: $F(3, 8) = 104.72$, $p < 0.001$; length: $F(3, 8) = 331.67$, $p < 0.001$), RGR-TO 2 (width: $F(3, 8) = 81.28$, $p < 0.001$; length: $F(3, 8) = 367.56$, $p < 0.001$), and RGR-TO 3 (width: $F(3, 8) = 92.82$, $p < 0.001$; length: $F(3, 8) = 374.17$, $p < 0.001$) can be revealed

by ANOVA. Significant differences between treatments ($p < 0.05$) can be confirmed by post hoc Tukey's HSD tests.

Strong positive correlations between the particle width and length can be revealed by correlation analysis within each RGR-TO sample. In RGR-TO 1, a correlation coefficient of r = 0.997 ($p < 0.01$) can be exhibited by the width and length, indicating a linear relationship between these variables. Similarly, high positive correlations between the width and length (r = 0.996, $p < 0.01$; r = 0.998, $p < 0.01$, respectively) can be demonstrated by RGR-TO 2 and RGR-TO 3.

Systematic changes in the particle size across treatments within each RGR-TO sample can be illustrated by trend analysis. Both the particle width and length can decrease progressively with increasing treatment intensity (0 to 9) in RGR-TO 1, RGR-TO 2, and RGR-TO 3. This trend suggests that high-pressure homogenization can lead to smaller particle sizes, indicating a dose-dependent effect on particle reduction.

High-pressure homogenization can effectively reduce the particle size in red ginseng residuals. ANOVA and correlation analyses within RGR-TO samples revealed significant variations in particle width and length and strong positive correlations between the two. Trend analysis suggests that the particle size decreases with increasing treatment intensity. The impact of treatment intensity on the particle size within RGR-TO samples was highlighted by the analysis, emphasizing the effectiveness of high-pressure homogenization in particle size reduction. Understanding these variations is crucial for optimizing manufacturing processes and applications in various industries. Further research is warranted to explore the underlying mechanisms driving these observed trends.

It has been observed that RGR-TO 3 had smaller particles compared to RGR-TO 2 and RGR-TO 1. Similarly, HPH 9 had smaller particles than HPH 6, 3, and 0, indicating a consistent trend. The smallest particle size was observed in RGR-TO 3 HPH 9. This trend has also been reported in the carboxymethylation of bleached rice hull, where increased DS and grinding resulted in a decreased particle size [54]. A study conducted in Australia on bagasse CNF using ball milling revealed a length of 2000 nm and a diameter of 50 nm [55]. TEMPO CNF from bleached kraft hardwood pulp had an original CNF width of 3.5 $\pm$ 2.0 nm and a length of 671.7 $\pm$ 961.2 nm. On the other hand, homogeneous CNF had a width of 2.0 $\pm$ 0.6 nm and a length of 639 $\pm$ 387.3 nm [43]. Furthermore, CNF from hardwood bleached kraft pulp provided by M company with a passed-through grinder (G) and high-pressure homogenizer (H) G2H4, G6H4, G8H4, and G8H10 showed a similar trend when using a nanoparticle analyzer (range size: 1.1–13.4 width and 36.7–266.7 length) and TEM (range size: 2.7–11.1 width and 99.1–669.1 length). The smallest size was observed in G8H10 [50].

Generally, smaller particles are more easily absorbed into the skin and can penetrate deeper into the inner layers [56]. This is because the skin has a natural protective barrier called the stratum corneum, which can prevent larger particles from entering [57]. By reducing the size of the active ingredient particles, they can more easily pass through this barrier and deliver their benefits more effectively [58]. Additionally, smaller particles can increase the surface area of the active ingredients, allowing for better contact with the skin and further enhancing their effectiveness [59]. Therefore, it is important to choose the smaller particle sizes to achieve optimal results.

4. Conclusions

RGR is primarily composed of glucose, with additional components such as galactose, arabinose, xylose, mannose, rhamnose, and uronic acid. Uronic acid is a highly sought-after ingredient in cosmetics due to its anti-aging, exfoliating, antioxidant, moisturizing, and pH-regulating properties. Through TEMPO-oxidation treatment, neutral monosaccharides in RGR were reduced while uronic acid content increased, making it an ideal active ingredient for cosmetics. The addition of carboxyl groups through TO oxidation in RGR-TO significantly improved its zeta potential, resulting in a stable nanomaterial dispersion with a zeta potential value above $\pm$30 mV. All RGR treated by TO had a zeta potential of more

than −40 mV, with RGR-TO 3 exhibiting the highest carboxylate content and the smallest particle size of nanofiber from RGR. By controlling the degree of oxidation pretreatment, RGR cellulose nanofibril with varied properties can be produced. This study demonstrates that TEMPO-oxidation pretreatment prior to nano fibrillation achieves this result.

Author Contributions: Performed the laboratory experiments and data analysis, A.Z. and V.G.F.; Investigation, A.Z. and V.G.F.; Validation, A.Z.; Writing—original draft, A.Z. and S.-J.S.; Writing—review and editing, S.-J.S. All authors have read and agreed to the published version of the manuscript.

Funding: This research was supported by the Chungbuk National University's Korea National University Development Project (2023)—2023100188.

Institutional Review Board Statement: Not applicable.

Data Availability Statement: The data presented in this study are available in the article.

Conflicts of Interest: All authors declare that the research was conducted in the absence of any commercial or financial relationships that could be construed as a potential conflict of interest.

References

1. Ahmed, M.B.; Zhou, J.L.; Ngo, H.H.; Guo, W.; Chen, M. Progress in the Preparation and Application of Modified Biochar for Improved Contaminant Removal from Water and Wastewater. *Bioresour. Technol.* **2016**, *214*, 836–851. [CrossRef]
2. Kim, D.; Park, M.; Haleem, I.; Lee, Y.; Koo, J.; Na, Y.C.; Song, G.; Lee, J. Natural product Ginsenoside 20 (S)-25-methoxyl-dammarane-3β, 12β, 20-triol in cancer treatment: A review of the pharmacological mechanisms and pharmacokinetics. *Front. Pharmacol.* **2020**, *11*, 521. [CrossRef]
3. Kim, Y.J.; Perumalsamy, H.; Castro-Aceituno, V.; Kim, D.; Markus, J.; Lee, S.; Kim, S.; Liu, Y.; Yang, D.C. Photoluminescent and self-assembled hyaluronic acid-zinc oxide-ginsenoside Rh2 nanoparticles and their potential caspase-9 apoptotic mechanism towards cancer cell lines. *Int. J. Nanomed.* **2019**, *2019*, 8195–8208. [CrossRef]
4. Wenli, S.; Shahrajabian, M.H.; Qi, C. Therapeutic roles of goji berry and ginseng in traditional Chinese. *J. Nutr. Food Secur.* **2019**, *4*, 293–305. [CrossRef]
5. Sengupta, P.; Dutta, S. Panax ginseng as reproductive medicine in male infertility: With a brief focus on herb-drug interaction. *Chem. Biol. Lett.* **2022**, *9*, 279.
6. Zhang, Z.; Zhou, Y.; Fan, H.; Billy, K.J.; Zhao, Y.; Zhan, X.; Yang, L.; Jia, Y. Effects of *Lycium barbarum* polysaccharides on health and aging of C. elegans depend on daf-12/daf-16. *Oxidative Med. Cell. Longev.* **2019**, *2019*, 6379493. [CrossRef]
7. Zhang, H.E.; Chu, M.Y.; Jiang, T.; Song, X.H.; Hou, J.F.; Cheng, L.Y.; Feng, Y.; Chen, C.B.; Wang, E.P. By-product of the red ginseng manufacturing process as potential material for use as cosmetics: Chemical profiling and in vitro antioxidant and whitening activities. *Molecules* **2022**, *27*, 8202. [CrossRef]
8. Payne, D. Skin integrity in older adults: Pressure-prone, inaccessible areas of the body. *Br. J. Community Nurs.* **2020**, *25*, 22–26. [CrossRef]
9. Meng, H.; Liu, X.K.; Li, J.R.; Bao, T.Y.; Yi, F. Bibliometric analysis of the effects of ginseng on skin. *J. Cosmet. Dermatol.* **2022**, *21*, 99–107. [CrossRef]
10. Jiménez, Z.; Kim, Y.J.; Mathiyalagan, R.; Seo, K.H.; Mohanan, P.; Ahn, J.C.; Kim, Y.J.; Yang, D.C. Assessment of radical scavenging, whitening and moisture retention activities of *Panax ginseng* berry mediated gold nanoparticles as safe and efficient novel cosmetic material. *Artif. Cells Nanomed. Biotechnol.* **2018**, *46*, 333–340. [CrossRef] [PubMed]
11. Shin, S.J.; Park, Y.H.; Jeon, S.G.; Kim, S.; Nam, Y.; Oh, S.M.; Lee, Y.Y.; Moon, M. Red ginseng inhibits tau aggregation and promotes tau dissociation in vitro. *Oxidative Med. Cell. Longev.* **2020**, *2020*, 7829842. [CrossRef]
12. Solano, F. Photoprotection and skin pigmentation: Melanin-related molecules and some other new agents obtained from natural sources. *Molecules* **2020**, *25*, 1537. [CrossRef]
13. Lakhan, M.K.; Lynch, M. Skin pigmentation. *Medicine* **2021**, *49*, 447–452. [CrossRef]
14. Hyun, S.H.; Kim, S.W.; Seo, H.W.; Youn, S.H.; Kyung, J.S.; Lee, Y.Y.; In, G.; Park, C.K.; Han, C.K. Physiological and pharmacological features of the non-saponin components in Korean Red Ginseng. *J. Ginseng Res.* **2020**, *44*, 527–537. [CrossRef]
15. Lee, S.M.; Bae, B.S.; Park, H.W.; Ahn, N.G.; Cho, B.G.; Cho, Y.L.; Kwak, Y.S. Characterization of Korean Red Ginseng (*Panax ginseng* Meyer): History, preparation method, and chemical composition. *J. Ginseng Res.* **2015**, *39*, 384–391. [CrossRef]
16. Kim, D.C.; In, M.J. Production of hydrolyzed red ginseng residue and its application to lactic acid bacteria cultivation. *J. Ginseng Res.* **2010**, *34*, 321–326. [CrossRef]
17. Huang, L.; Ren, C.; Li, H.J.; Wu, Y.C. Recent progress on processing technologies, chemical components, and bioactivities of Chinese red ginseng, American red ginseng, and Korean red ginseng. *Food Bioprocess Technol.* **2022**, *15*, 47–71. [CrossRef]
18. Ji, X.; Hou, C.; Shi, M.; Yan, Y.; Liu, Y. An insight into the research concerning Panax ginseng CA Meyer polysaccharides: A review. *Food Rev. Int.* **2022**, *38*, 1149–1165. [CrossRef]

19. Lee, J.W.; Do, J.H. Extraction condition of acidic polysaccharide from Korean red ginseng marc. *J. Ginseng Res.* **2002**, *26*, 202–205. [CrossRef]
20. Khalil, H.A.; Davoudpour, Y.; Islam, M.N.; Mustapha, A.; Sudesh, K.; Dungani, R.; Jawaid, M. Production and modification of nanofibrillated cellulose using various mechanical processes: A review. *Carbohydr. Polym.* **2014**, *99*, 649–665. [CrossRef]
21. Beck, S.; Bouchard, J.; Berry, R. Dispersibility in water of dried nanocrystalline cellulose. *Biomacromolecules* **2012**, *13*, 1486–1494. [CrossRef]
22. Ma, H.; Zhou, B.; Li, H.S.; Li, Y.Q.; Ou, S.Y. Green composite films composed of nanocrystalline cellulose and a cellulose matrix regenerated from functionalized ionic liquid solution. *Carbohydr. Polym.* **2011**, *84*, 383–389. [CrossRef]
23. Frone, A.N.; Panaitescu, D.M.; Donescu, D. Some aspects concerning the isolation of cellulose micro-and nano-fibers. *UPB Bul. Stiintific Ser. B Chem. Mater. Sci.* **2011**, *73*, 133–152.
24. Ferrer, A.; Filpponen, I.; Rodríguez, A.; Laine, J.; Rojas, O.J. Valorization of residual Empty Palm Fruit Bunch Fibers (EPFBF) by microfluidization: Production of nanofibrillated cellulose and EPFBF nanopaper. *Bioresour. Technol.* **2012**, *125*, 249–255. [CrossRef]
25. Siró, I.; Plackett, D. Microfibrillated cellulose and new nanocomposite materials: A review. *Cellulose* **2010**, *17*, 459–494. [CrossRef]
26. Frone, A.N.; Panaitescu, D.M.; Donescu, D.; Spataru, C.I.; Radovici, C.; Trusca, R.; Somoghi, R. Preparation and characterization of PVA composites with cellulose nanofibers obtained by ultrasonication. *BioResources* **2011**, *6*, 487–512. [CrossRef]
27. Henriksson, M.; Berglund, L.A. Structure and properties of cellulose nanocomposite films containing melamine formaldehyde. *J. Appl. Polym. Sci.* **2007**, *106*, 2817–2824. [CrossRef]
28. Hubbe, M.A.; Rojas, O.J.; Lucia, L.A.; Sain, M. Cellulosic nanocomposites: A review. *BioResources* **2008**, *3*, 929–980. [CrossRef]
29. Ifuku, S.; Nogi, M.; Abe, K.; Handa, K.; Nakatsubo, F.; Yano, H. Surface modification of bacterial cellulose nanofibers for property enhancement of optically transparent composites: Dependence on acetyl-group DS. *Biomacromolecules* **2007**, *8*, 1973–1978. [CrossRef]
30. Saito, T.; Hirota, M.; Tamura, N.; Kimura, S.; Fukuzumi, H.; Heux, L.; Isogai, A. Individualization of nano-sized plant cellulose fibrils by direct surface carboxylation using TEMPO catalyst under neutral conditions. *Biomacromolecules* **2009**, *10*, 1992–1996. [CrossRef]
31. Moud, A.A. Advanced cellulose nanocrystals (CNC) and cellulose nanofibrils (CNF) aerogels: Bottom-up assembly perspective for production of adsorbents. *Int. J. Biol. Macromol.* **2022**, *222*, 1–29. [CrossRef]
32. Ok, S.; Kang, J.S.; Kim, K.M. Simultaneous analysis method for polar and non-polar ginsenosides in cultivated wild ginseng by reversed-phase HPLC-CAD. *J. Life Sci.* **2016**, *26*, 247–252. [CrossRef]
33. Baek, S.H.; Bae, O.N.; Park, J.H. Recent methodology in ginseng analysis. *J. Ginseng Res.* **2012**, *36*, 119. [CrossRef]
34. *ISO 22412:2008*; Particle Size Analysis—Dynamic Light Scattering (DLS). International Organization for Standardization: Geneva, Switzerland, 2008.
35. Wu, C.; McClements, D.J.; He, M.; Fan, Z.; Li, Y.; Teng, F. Preparation of okara cellulose hydrogels using ionic liquids: Structure, properties, and performance. *J. Mol. Liq.* **2021**, *331*, 115744. [CrossRef]
36. Merkx, D.W.; Westphal, Y.; van Velzen, E.J.; Thakoer, K.V.; de Roo, N.; van Duynhoven, J.P. Quantification of food polysaccharide mixtures by 1H NMR. *Carbohydr. Polym.* **2018**, *179*, 379–385. [CrossRef] [PubMed]
37. de Souza, A.C. Quantification of Food Polysaccharides by means of NMR. In *Modern Magnetic Resonance*; Springer: Cham, Switzerland, 2017. [CrossRef]
38. Delattre, C.; Pierre, G.; Gardarin, C.; Traïkia, M.; Elboutachfaiti, R.; Isogai, A.; Michaud, P. Antioxidant activities of a polyglucuronic acid sodium salt obtained from TEMPO-mediated oxidation of xanthan. *Carbohydr. Polym.* **2015**, *116*, 34–41. [CrossRef]
39. Srihirun, S. Development of 3D-Microfluidic Paper-Based Analytical Devices for Determination of Gluconic Acid in Skincare Products. Master's Thesis, Srinakharinwirot University, Bangkok, Thailand, 2020. Available online: http://ir-ithesis.swu.ac.th/dspace/bitstream/123456789/576/1/gs611110186.pdf (accessed on 12 September 2023).
40. Lee, G.S.; Kim, J.W.; Lee, C.I.; Pyo, H.B.; Lee, K.J. Application of Glucuronic Acid with New Cosmetic Active Ingredient. *J. Soc. Cosmet. Sci. Korea* **2004**, *30*, 471–477.
41. Tian, L.; Zhao, Y.; Guo, C.; Yang, X. A comparative study on the antioxidant activities of an acidic polysaccharide and various solvent extracts derived from herbal Houttuynia cordata. *Carbohydr. Polym.* **2011**, *83*, 537–544. [CrossRef]
42. Hasanin, M.S.; Mostafa, A.M.; Mwafy, E.A.; Darwesh, O.M. Eco-friendly cellulose nano fibers via first reported Egyptian Humicola fuscoatra Egyptia X4: Isolation and characterization. *Environ. Nanotechnol. Monit. Manag.* **2018**, *10*, 409–418. [CrossRef]
43. Zhai, L.; Kim, H.C.; Kim, J.W.; Kim, J. Simple centrifugal fractionation to reduce the size distribution of cellulose nanofibers. *Sci. Rep.* **2020**, *10*, 11744. [CrossRef]
44. Masruchin, N.; Amanda, P.; Kusumaningrum, W.B.; Suryanegara, L.; Nuryawan, A. Particle size distribution and yield analysis of different charged cellulose nanofibrils obtained by TEMPO-mediated oxidation. In *IOP Conference Series: Earth and Environmental Science*; IOP Publishing: Bogor, Indonesia, 2020; Volume 572, p. 012045. [CrossRef]
45. Clogston, J.D.; Patri, A.K. Zeta potential measurement. In *Characterization of Nanoparticles Intended for Drug Delivery*; Humana Press: Totowa, NJ, USA, 2011; pp. 63–70. [CrossRef]
46. Zahra, A.; Lim, S.K.; Shin, S.J.; Yeon, I.J. Properties of Green Tea Waste as Cosmetics Ingredients and Rheology Enhancers. *Appl. Sci.* **2022**, *12*, 12871. [CrossRef]
47. Lal, S.S.; Mhaske, S.T. TEMPO-oxidized cellulose nanofiber/kafirin protein thin film crosslinked by Maillard reaction. *Cellulose* **2019**, *26*, 6099–6118. [CrossRef]

48. Li, X.; Li, J.; Kuang, Y.; Guo, S.; Mo, L.; Ni, Y. Stabilization of Pickering emulsions with cellulose nanofibers derived from oil palm fruit bunch. *Cellulose* **2020**, *27*, 839–851. [CrossRef]
49. Liao, J.; Pham, K.A.; Breedveld, V. Rheological characterization and modeling of cellulose nanocrystal and TEMPO-oxidized cellulose nanofibril suspensions. *Cellulose* **2020**, *27*, 3741–3757. [CrossRef]
50. Song, W.; Juhn, S.; Gwak, J.H.; Shin, S.J.; Seong, H.A. Width and Length Measurement of Cellulose Nanofibril by Nanoparticle Analyzer: Comparison with TEM Image Analysis. *J. Korea TAPPI* **2019**, *51*, 121–127. [CrossRef]
51. Balea, A.; Blanco, A.; Delgado-Aguilar, M.; Monte, M.C.; Tarres, Q.; Fuente, E.; Mutje, P.; Negro, C. Nanocellulose characterization challenges. *BioResources* **2021**, *16*, 4382. [CrossRef]
52. Iwamoto, S.; Lee, S.H.; Endo, T. Relationship between aspect ratio and suspension viscosity of wood cellulose nanofibers. *Polym. J.* **2014**, *46*, 73–76. [CrossRef]
53. Han, J.; Zhou, C.; Wu, Y.; Liu, F.; Wu, Q. Self-assembling behavior of cellulose nanoparticles during freeze-drying: Effect of suspension concentration, particle size, crystal structure, and surface charge. *Biomacromolecules* **2013**, *14*, 1529–1540. [CrossRef]
54. Cao, X.; Lim, S.K.; Song, W.Y.; Shin, S.J.; Seong, H.A. Impact of carboxymethylation pretreatment on bleached rice hull nanofiber by grinding. *J. Korea TAPPI* **2021**, *53*, 146–156. [CrossRef]
55. Sofla, M.R.K.; Brown, R.J.; Tsuzuki, T.; Rainey, T.J. A comparison of cellulose nanocrystals and cellulose nanofibres extracted from bagasse using acid and ball milling methods. *Adv. Nat. Sci. Nanosci. Nanotechnol.* **2016**, *7*, 035004. [CrossRef]
56. Nafisi, S.; Maibach, H.I. Skin penetration of nanoparticles. In *Emerging Nanotechnologies in Immunology*; Elsevier: Amsterdam, The Netherlands, 2018; pp. 47–88. [CrossRef]
57. Prausnitz, M.R.; Elias, P.M.; Franz, T.J.; Schmuth, M.; Tsai, J.C.; Menon, G.K.; Holleran, W.M.; Feingold, K.R. Skin barrier and transdermal drug delivery. *Dermatology* **2012**, *3*, 2065–2073.
58. McClements, D.J. Encapsulation, protection, and delivery of bioactive proteins and peptides using nanoparticle and microparticle systems: A review. *Adv. Colloid Interface Sci.* **2018**, *253*, 1–22. [CrossRef] [PubMed]
59. Prow, T.W.; Grice, J.E.; Lin, L.L.; Faye, R.; Butler, M.; Becker, W.; Wurm, E.M.; Yoong, C.; Robertson, T.A.; Soyer, H.P.; et al. Nanoparticles and microparticles for skin drug delivery. *Adv. Drug Deliv. Rev.* **2011**, *63*, 470–491. [CrossRef] [PubMed]